Nanoscale

ROYAL SOCIETY OF CHEMISTRY

PAPER

View Article Online
View Journal

Cite this: DOI: 10.1039/d0nr04899b

Single-domain antibody C7b for address delivery of nanoparticles to HER2-positive cancers†

Yuri A. Vorotnikov, [a] Evgeniya D. Novikova,[a] Anastasiya O. Solovieva,[b] Daniil V. Shanshin,[c] Alphiya R. Tsygankova, [a] Dmitrii N. Shcherbakov,[c,f] Olga A. Efremova *[b,d,e] and Michael A. Shestopalov *[a]

Received 30th June 2020,
Accepted 29th September 2020

DOI: 10.1039/d0nr04899b

rsc.li/nanoscale

Monoclonal antibodies (mAb) demonstrate great potential as immunotherapy agents for the treatment of diseases such as cancer as well as tagging for the targeted delivery of multicomponent therapeutic or diagnostic systems. Nevertheless, the large physical size, poor stability of mAbs and abnormal allergic reactions still remain the main issues affecting their generalised use. Single-domain antibodies (sdAb) are seen as the next generation of antibody derived therapeutics and diagnostics. This work presents the optimised production method for HER2-specific sdAb C7b, which led to an ~11-fold increase in protein yield. In addition, the *in vitro* and *in vivo* efficiencies of the targeted delivery of a model nanoparticle cargo (50 nm silica particles doped with Mo_6 phosphorescent clusters) conjugated to C7b against those conjugated to HER2-specific trastuzumab is benchmarked. Specifically, this paper demonstrates the significantly higher rate of accumulation in and excretion from xenograft cancer tissue of nanoparticles with C7b, which is of particular importance for diagnostics, *i.e.* delivery of imaging agents.

Introduction

Within the past several decades, the clinical utilisation of monoclonal antibodies (mAbs) against cancer-related transmembrane receptors or their ligands has become more common.[1,2] mAbs are already clinically used as therapeutic agents for specific types of cancer; *e.g.* trastuzumab (Herceptin®) is used to treat some types of breast cancer, oesophageal cancer and stomach cancer and alemtuzumab (Campath®) is used against chronic lymphocytic leukaemia. mAbs are also used as a part of complex therapies; *e.g.* ibritumomab tiuxetan (Zevalin®) as an example of a radiolabelled mAb. Finally, mAbs are also widely studied for their application in targeted delivery of new therapeutic and diagnostics agents, *e.g.* PET/SPECT or optical imaging agents,[3,4] agents for photothermal, photodynamic and chemotherapy,[1,5–8] *etc*. However, there are concerns over the tumour penetration of mAbs due to their significant size (~150 kDa), which may be increased even further after conjugation with a nanoparticle-based drug or imaging agent; secondly, over the long half-life of several days, which is good from the therapeutic point of view but a challenge from a diagnostics perspective, and, thirdly, over the adverse immune responses of patients.[1,2]

Variable domains of heavy-chain antibodies from the Camelidae family of animals and single-domain antibodies (sdAb), *aka* nanobodies, were recently suggested as the next generation of antibody derived immuno-oncology therapeutics as they may provide an answer to several of the above concerns.[2,9–11] Indeed, they retain their full antigen binding potential, while they cause noticeably weaker immune response due to their high similarity with human immunoglobulin heavy chain (VH) sequences. In addition, due to smaller size (~10–15 kDa), they have better penetration into solid tumours (*i.e.* can improve drug delivery efficiency)[1,11] and thus access the tumour cells. To add to their benefits, the nanobodies have higher solubility and higher thermal and chemical stability than full-size human/humanised mAbs and the fact that they can be easily manufactured in large quantities in microorganisms makes them really attractive for numerous applications in fundamental research, diagnostics and therapy.[1,9–11]

[a]*Nikolaev Institute of Inorganic Chemistry SB RAS, 3 Acad. Lavrentiev ave., 630090 Novosibirsk, Russian Federation. E-mail: shtopy@niic.nsc.ru*
[b]*Research Institute of Clinical and Experimental Lymphology – branch of ICG SB RAS, 2 Timakova str., 630060 Novosibirsk, Russian Federation*
[c]*State Research Center of Virology and Biotechnology VECTOR, Koltsovo, 630559 Novosibirsk Oblast, Russian Federation*
[d]*The Federal Research Center of Fundamental and Translational Medicine, 2 Timakova str., 630117 Novosibirsk, Russian Federation*
[e]*Department of Chemistry and Biochemistry, University of Hull, Cottingham Road, Hull, HU6 7RX, UK*
[f]*Russian-American Anti-Cancer Center, Altai State University, 61 Lenina ave., 656049, Barnaul, Russian Federation*

†Electronic supplementary information (ESI) available. See DOI: 10.1039/d0nr04899b

sdAb C7b (C7b) [GenBank: AFN61318.1] is one of the relatively recently isolated llama antibodies specific to human epidermal growth factor receptor 2 (HER2 receptor),[12] which is overexpressed in approximately 15–30% of breast cancers and 10–30% of gastric/gastroesophageal cancers, as well as some other cancers of the ovaries, endometrium, bladder, lung, colon, and head and neck.[13] sdAb C7b can be thus considered as an alternative to trastuzumab, which is a recombinant humanised mAb specific to HER2; however, so far, in the literature, there are only a couple of studies.[12,14]

In this work we, firstly, report on a significant improvement of the conventional method for the production of sdAb C7b by the optimisation of the codon composition of the C7b nucleotide sequence and the addition of the expressivity tag T7 to the N-terminus of the protein. This resulted in a ~11-fold increase in the antibody yield compared to the originally published method.[12,14] Secondly, we benchmark the targeted delivery of nanoparticles conjugated to C7b against those conjugated to commercial trastuzumab both *in vitro* and *in vivo*.

Silica nanoparticles doped by Mo_6 clusters ($\{Mo_6I_8\}$@SiO_2 NPs) were chosen as cargo since they have profound luminescence properties in the red/near-infrared region and thus the *in vitro* delivery can be easily monitored by conventional optical methods without the need for extra labelling. We have already showcased the utilisation of molybdenum cluster-doped microparticles (500 nm) as a trackable agent for protein transduction into Hep-2 cells (human epidermoid larynx carcinoma),[15] while another group used similar nanoparticles (but doped with $[\{Mo_6I_8\}(C_2F_5COO)_6]^{2-}$) to demonstrate that their uptake by SKmel 28 cells (human melanoma) could be enhanced, when they are conjugated to human transferrin.[16] Herein, we use luminescent Mo_6 cluster-doped silica nanoparticles, $\{Mo_6I_8\}$@SiO_2 NPs, which have a size of 50 nm as a labelling model. Namely, we report on the comparative study of the cellular toxicity and uptake rate of $\{Mo_6I_8\}$@SiO_2 NPs conjugated with a nanobody C7b or with trastuzumab on the cell lines SKBR3 (human breast cancer) and Hep-2 cells, which have a high and low level of HER2 expression, respectively. We also tested the permeation of both conjugates into the solid tumour SKBR3 cancer xenograft and assessed the phototoxicity of the conjugate to the cancerous tissue.

Experimental section

Chemicals

All reagents and solvents were purchased from Alfa Aesar, Sigma Aldrich or Fluka and were used as received without further purification. $(Bu_4N)_2[\{Mo_6I_8\}(NO_3)_6]$ was synthesised according to the described procedures.[17] $\{Mo_6I_8\}$@SiO_2 nanoparticles with an average size of 50 nm were prepared according to the previously reported method.[18] Trastuzumab (Herceptine®) was offered by the Lymphology Institute Clinic, Novosibirsk, Russia.

Cell lines

The human larynx carcinoma cell line (Hep-2) was purchased from the State Research Center of Virology and Biotechnology VECTOR. The human breast cancer cell line (SKBR3) was provided by the N.N. Blokhin National Medical Research Centre of Oncology of the Health Ministry of Russia. The Hep-2 cells were cultured in Eagle's Minimum Essential Medium (MEM, pH = 7.4, Sigma Aldrich, USA) and the SKBR3 cells in Roswell Park Memorial Institute (RPMI, Sigma Aldrich, USA) 1640 Medium supplemented with a 10% fetal bovine serum (FBS, Gibco, USA) under a humidified atmosphere (5% CO_2 and 95% air) at 37 °C.

Single-domain antibody C7b preparation

Obtaining recombinant plasmid pET21a-C7b. The synthesis of a gene encoding a single-domain antibody (sdAb) C7b [GenBank: AFN61318.1] was performed by "DNA Synthesis", Russia. In order to increase the synthesis efficiency, the codon composition of the nucleotide sequence encoding sdAb C7b was optimised using EFM Calculator and GeneOptimizer.[19–21] In addition, the expressivity tag T7 was added to the N-terminal part of the C7b antibody. The synthesised sequence encoding sdAb C7b and the pET21a expression vector were then digested by restriction enzymes NdeI-XhoI (New England Biolabs, UK). *E. coli* cells of Stbl3 strain (Thermo Fisher Scientific, USA) were transformed by recombinant plasmid pET21-C7b-CO through chemical transformation.[22] *E. coli* cells were plated on a selective medium containing LB agar and 100 μg mL^{-1} of ampicillin and used for plasmid producing. The recombinant plasmid was verified by nucleotide sequencing.

Production and purification of sdAb C7b. *E. coli* cells of the strain BL21 (DE3) (Promega, USA) were used for the expression of sdAb C7b. The transformation of competent cells with plasmid pET21-C7b-CO was performed by chemical means.[22] Isopropyl-β-D-1-thiogalactopyranoside (IPTG, 1 mM) was used as an inductor. The induction process was carried out as follows: fresh LB medium was inoculated with a producer strain containing the plasmid pET21-C7b-CO in the ratio of 1 : 100 and incubated in a thermostatic rotary type shaker at 180 rpm and +37 °C until OD_{600} reached 0.6–0.8. Subsequently, 1 mM IPTG was added to induce expression. Incubation was carried out for 16 hours followed by the precipitation of the cells by centrifugation.

Protein synthesis was controlled by the Laemmli-SDS-PAGE method.[23] An aliquot of the culture medium for analysis was collected before the addition of the inducer, as well as 1 hour, 2 hours and 4 hours after the addition of the inducer.

Purification of sdAb C7b was performed using metal-chelate affinity chromatography on a Ni-IMAC Sepharose sorbent (GE Healthcare, USA). The cells were harvested by centrifugation at 4000 rpm for 10 min at 4 °C, followed by their resuspension in lysis buffer (30 mM of NaH_2PO_4, 20 mM of imidazole, 500 mM of NaCl, 0.1% Triton X100, pH 7.4) by ultrasound for 10 cycles of 90 s with breaks of 3 minutes on

ice. The cell lysate was purified from debris by centrifugation at 15 000*g* for 25 min at +4 °C. During the chromatography, the binding of the C7b antibody to the sorbent occurred at a flow rate of 1.5 mL min^{-1}. The column was then washed to remove unbound proteins with five column volumes of wash buffer (30 mM of NaH_2PO_4, 40 mM of imidazole, 500 mM of NaCl, and pH 7.4) at a flow rate of 2 mL min^{-1}. C7b was eluted with three column volumes of an elution buffer (30 mM of NaH_2PO_4, 500 mM of imidazole, 500 of mM NaCl, and pH 7.4) at a flow rate of 1 mL min^{-1}. Fractions of 5 mL were collected and the concentration of C7b was determined using a NanoPhotometer NP80 (Implen, Germany). The production yield calculated per litre of culture medium was ~210–220 mg L^{-1}. The final concentration of C7b was 3.4 mg mL^{-1}.

Preparation of $\{Mo_6I_8\}$@SiO_2 nanoparticles

Nanoparticles $\{Mo_6I_8\}$@SiO_2 with an average particle size of 50 nm were synthesised according to an earlier described method.[18] In general, $(Bu_4N)_2[\{Mo_6I_8\}(NO_3)_6]$ (17 mg, 0.007 mmol) dissolved in ethanol (2.5 mL) was added to distilled water (2.5 mL). To prepare a microemulsion, both the ethanol/water solution of $(Bu_4N)_2[\{Mo_6I_8\}(NO_3)_6]$ (1.6 mL) and 25% aqueous ammonia solution (1.3 mL) were added to the mixture of *n*-heptane (47 mL) and Brij L4 surfactant (15 mL). This mixture was stirred for 30 min to ensure the homogeneity of the microemulsion. Finally, tetraethyl orthosilicate (2 mL) was added and the mixture was stirred for 72 h. Thereafter, the obtained yellowish colloidal solution was centrifuged (7000 rpm for 10 min), washed successively with ethanol, water and acetone and dried at 60 °C in air. The 50 nm size and spherical shape of the particles were confirmed using transmission electron microscopy (TEM) on a Libra 120 (Zeiss) TEM (Fig. S1†).

ICP analysis of $\{Mo_6I_8\}$@SiO_2

Prior to their analysis, the samples of dried nanoparticles were dissolved in a mixture of HNO_3 : HF = 1 : 1 at elevated temperature on a water bath. Molybdenum content in the samples was determined using a high-resolution spectrometer iCAP-6500 (Thermo Scientific) with a cyclone-type spray chamber and "SeaSpray" nebuliser. The spectra were obtained with axial plasma viewing. The standard operating conditions of the ICP-AES system were as follows: power – 1150 W, injector inner diameter – 3 mm, carrier argon flow – 0.7 L min^{-1}, accessorial argon flow – 0.5 L min^{-1}, cooling argon flow – 12 L min^{-1}, number of the parallel measurements – 3 and integration time – 5 s. Deionised water ($R \approx 18$ MΩ) was used to prepare sample solutions. All chemical reagents were of analytical grade. The mass content (ω) of $\{Mo_6I_8\}$-units was calculated from the ω of Mo using the formula:

$$\omega_{\{Mo_6I_8\}} = \frac{6\omega_{Mo}M_{\{Mo_6I_8\}}}{M_{Mo}}$$

where ω_{Mo} is the mass content of molybdenum in the sample, $M_{\{Mo6I8\}}$ is the molar mass of $\{Mo_6I_8\}$ unit (1590.88 mol g^{-1}), and M_{Mo} is the molar mass of Mo (95.94 mol g^{-1}).

Preparation of glycidyl-modified $\{Mo_6I_8\}$@SiO_2 nanoparticles (glycidyl-$\{Mo_6I_8\}$@SiO_2)

50 mg of powdered $\{Mo_6I_8\}$@SiO_2 NPs was dispersed in 2.5 mL of hexane by sonication for 30 min. 0.0075 mL of Et_3N and 0.05 mL of (3-glycidyloxypropyl)trimethoxysilane were then added to the dispersion and the resultant mixture was heated at 55 °C for 3.5 h under gentle stirring. The reaction product, *i.e.* glycidyl-$\{Mo_6I_8\}$@SiO_2 nanoparticles, was then separated by centrifugation at 7000 rpm for 10 min and washed five times with hexane and one time with acetone by sonication/centrifugation cycles and finally dried at ambient conditions.

Conjugation of glycidyl-$\{Mo_6I_8\}$@SiO_2 nanoparticles with sdAb C7b ($\{Mo_6I_8\}$@SiO_2-C7b) or trastuzumab ($\{Mo_6I_8\}$@SiO_2-trastuzumab)

10 mg of glycidyl-$\{Mo_6I_8\}$@SiO_2 was washed twice with 5 mL of buffer solution (0.1 M NaCl) and re-suspended in 1 mL of the coupling buffer (Na_2CO_3 and $NaHCO_3$ in the concentrations 5.8 mg mL^{-1} and 3.8 mg mL^{-1}, respectively, giving a final pH = 10). 1 or 2 mL of C7b (3.4 mg mL^{-1}) or trastuzumab (3.4 mg mL^{-1}) was added to the dispersion of glycidyl-$\{Mo_6I_8\}$@SiO_2 and gently stirred for 24 h. Thereafter, the resultant dispersions were washed with 5 mL of buffer solution, re-suspended in 2 mL of the quenching solution (glycine : Triton X-100 : d/d water = 50 mg : 0.014 mL : 20 mL) and mixed gently for 30 min. Finally, the conjugates were washed again with 5 mL of the buffer solution and resuspended in 1 mL of storage buffer (Triton X-100 : phosphate-buffered saline (PBS) = 0.023 mL : 50 mL having final pH = 7.4). The final concentration of the conjugates was 10 mg mL^{-1}.

Dot blot assay. The reactivity of sdAb C7b and conjugate $\{Mo_6I_8\}$@SiO_2-C7b was evaluated using a dot blot assay. The recombinant human ErbB2/HER2 Fc Chimera Protein (50 ng) (R&D Systems) was absorbed into the nitrocellulose membrane (Hybond-C Extra). To eliminate nonspecific binding, the membrane surface was treated with a 1% BSA solution in PBS-0.1% Tween (PBS-T), followed by three washings with PBS-T. The membrane surface was then treated with 1 or 2 μL of C7b (3.4 μg and 6.7 μg) or 1 μL of the conjugates (C7b weight in conjugates was equal to 3.4 μg and 6.7 μg) dispersed in the solution of 1% BSA in PBS-T followed by 10 min incubation and three washings with PBS-T. To determine the antigen–antibody and antigen–conjugate complex, the monoclonal HHHHHH epitope tag (#1706520, Sigma-Aldrich, USA) in a 1% solution of BSA in PBS was added and followed by 10 min incubation and three washings with PBS-T. To detect antigen–antibody interaction, the membrane was treated with goat anti-mouse antibodies labelled with alkaline phosphatase (BIORAD) in a dilution recommended by the manufacturer, followed by 10 min incubation and washing with PBS-T. Aqueous solutions of 5-bromo-4-chloro-3-indolyl phosphate (BCIP) and nitro blue tetrazole (NBT) in a dilution recommended by the manufacturer were used as a substrate for alkaline phosphatase. The enzymatic reaction was stopped by washing with distilled water.

Enzyme-linked immunosorbent assay (ELISA). Plate wells were sensitised with purified sdAb C7b and its conjugate with the initial concentration of 6.7 mg_{C7b} mL^{-1} in dilution from 1/100 (67 μg_{C7b} mL^{-1}) with a 2-fold step up to 1/204 800 dilution (3.3 ng_{C7b} mL^{-1}) in Tris-buffered saline (TBS, 0.15 M of NaCl, 0.02 M of Tris·HCl, pH = 7.4) at +22 °C for 18 hours. After washing with a mixture of TBS and Tween 20 (0.05%) (TBS-T) three times, the plates were treated with 1% casein in TSB-T and incubated for 1 h at +37 °C. The casein solution was then removed and 50 μL of the recombinant human ErbB2/HER2 Fc (5 ng per well) was added and the wells were incubated for 1 h at +37 °C. After washing with TSB-T for three times, anti-human IgG (whole molecule)–peroxidase antibodies produced in goats (A8667, Sigma-Aldrich, USA) were added in the dilution according to the manufacturer's recommendation and the wells were incubated for 1 h at +37 °C. After washing the wells with TSB-T three times, the substrate solution containing 0.1 mg mL^{-1} of TMB (3.3′,5.5′-tetramethylbenzidine, Sigma-Aldrich, USA) and the buffer for the substrate oxidation containing 0.02% H_2O_2 were added. The plates were incubated under dark conditions for 15–20 minutes at room temperature. The enzymatic reaction was stopped by the addition of 1 M HCl and after 2–4 min, the optical density was measured using a Uniscan spectrophotometer (Finland) at λ = 450 nm.

Luminescence

The luminescence spectra were recorded for aqueous dispersions of all samples. The samples were excited by 355 nm laser pulses (6 ns duration, LOTIS TII, LS-2137/3). The corrected emission spectra were recorded using a red-light-sensitive multichannel photodetector (Hamamatsu Photonics, PMA-12). The luminescence lifetime and quantum yields were determined for powdered samples of original nanoparticles $\{Mo_6I_8\}$@SiO_2 and modified glycidyl-$\{Mo_6I_8\}$@SiO_2 nanoparticles. All samples were placed between two non-fluorescent glass plates. The measurements were carried out at 298 K. For emission decay measurements, the emission was analysed using a streakscope system (Hamamatsu Photonics, C4334 and C5094). The emission quantum yields were determined using an absolute photoluminescence quantum yield measurement system (Hamamatsu Photonics, C9920-03), which comprises a xenon light excitation source (the excitation wavelength was 380 nm), an integrating sphere, and a red-sensitive multichannel photodetector (Hamamatsu Photonics, PMA-12).

Cytotoxicity

The effect of $\{Mo_6I_8\}$@SiO_2-C7b and $\{Mo_6I_8\}$@SiO_2-trastuzumab on the Hep-2 and SKBR3 cell metabolic activity was determined using the 3-[4,5-dimethylthiazol-2-yl]-2,5-diphenyltetrazolium bromide (MTT) colorimetric assay. The cell cultures were seeded into 96-well plates at 7×10^3 cells per well in a medium containing $\{Mo_6I_8\}$@SiO_2-C7b or $\{Mo_6I_8\}$@SiO_2-trastuzumab with concentrations ranging from 10 to 500 μg mL^{-1} and then incubated for 72 h under a 5% CO_2 atmosphere. 5 μL of the MTT solution (5 mg mL^{-1}) was added to each well, and the plates were incubated for a further 4 h. The formazan produced was then dissolved in DMSO (100 μL). The optical density of the solutions was measured using a Multiskan FC plate reader (Thermo Fisher Scientific, USA) at a wavelength of 570 nm. The experiment was repeated on three separate days.

Cellular internalisation assay

For the confocal laser scanning microscopy, Hep-2 and SKBR3 cells were seeded on slides (1×10^5 cells per slide) and incubated overnight. The medium was then replaced with a fresh medium containing 0.1 mg mL^{-1} of $\{Mo_6I_8\}$@SiO_2-C7b and $\{Mo_6I_8\}$@SiO_2-trastuzumab and incubated for 24 h. Finally, the cells were washed twice with PBS, fixed in 4% paraformaldehyde, and visualised using a Zeiss LSM 510 confocal microscope (Carl Zeiss Inc., Jena, Germany) equipped with a laser diode (405 nm) for fluorescence. The images were obtained and analysed with the ZEN 2009 software.

Animals and housing conditions

The *in vivo* studies were approved by the Ethics Committee of the RICEL-branch of ICG SB RAS (No. 140 dated 26.04.2018). All animal procedures were carried out in accordance with the protocols approved by the Bioethics Committee of the Siberian Branch of the Russian Academy of Sciences, recommendations for the proper use and care of laboratory animals (European Communities Council Directive 86/609/CEE) and the principles of the Declaration of Helsinki. The mice were housed in stainless plastic cages containing sterile sawdust as bedding in ventilated animal rooms with free access to water and a commercial laboratory complete food.

Tumour xenotransplantation in Nu/J mice

To establish a tumour xenograft model, 9 female Nu/J mice at 8 weeks were inoculated subcutaneously on their lateral thigh with 3×10^6 SKBR3 cells per mice. Tumour-bearing mice were randomly allocated into 3 groups and the treatments were commenced when the average tumour size reached 1 × 0.5 × 0.5 cm.

Conjugate quantification in tumour xenografts

Prior to experiments with xenograft mice, the tolerance of subcutaneous administration of nanoparticles was investigated on model female Balb/C mice. 0.7 mL (C = 5 mg mL^{-1}) of suspension of $\{Mo_6I_8\}$@SiO_2, $\{Mo_6I_8\}$@SiO_2-trastuzumab or $\{Mo_6I_8\}$@SiO_2-C7b was injected subcutaneously in the medial thigh area of 3 mice. After the injection, the animals did not demonstrate any symptoms of intoxication and behaved normally.

Thereafter, 9 female mice of Nu/J line with xenograft were injected with either neat $\{Mo_6I_8\}$@SiO_2 (negative control, C = 5 mg mL^{-1}) or with the conjugates $\{Mo_6I_8\}$@SiO_2-C7b or $\{Mo_6I_8\}$@SiO_2-trastuzumab (positive control, C = 5 mg mL^{-1}) subcutaneously around the tumour by 7 consecutive injections with the dose of 0.1 mg each. The total volume injected was 0.7 mL and the total dose was 3.5 mg. The mice were sacrificed after 1, 3 and 24 hours from sample administration, and the quantity of the nanoparticles in tumour xenografts was determined using the ICP-AES technique by monitoring the content

of silicon atoms in the tissue. Concentrations obtained were normalised to 1 g of the weight of the tissue sample.

Photodynamic activity assessment *in vivo*

A female mouse of Nu/J line with an SKBR3 tumour xenograft (solid ellipsoidal shape and size 1.0 × 0.5 × 0.5 cm) was injected with $\{Mo_6I_8\}$@SiO_2-C7b dispersion (C = 5 mg mL^{-1}) subcutaneously around the tumour by 7 consecutive injections with the dose of 0.1 mg each. After 1 hour (*i.e.* at the maximum accumulation), the tumour was irradiated with a halogen lamp (500 W, λ = ~400–700 nm) at a distance of 50 cm for 30 minutes. The procedure was repeated twice more at an interval of 3 days.

Results and discussion

Optimisation of the method of sdAb C7b preparation

The practical application of any monoclonal antibody requires its availability in sufficient quantities. In the original method,[12] the target C7b antibodies were obtained by immunizing llamas with HER2-expressing ovarian cancer cell line SKOv3, followed by the isolation of the target antibodies from the resulting library. This method is, thus, time-consuming, costly and not suitable for the production of antibodies on an industrial scale. Therefore, we were keen to develop a more conventional system for the production of sdAb C7b in higher yields. Due to advantages such as the high rate of target protein production and the well-established genetics,[24] the widely used *E. coli* bacteria system was chosen as an expression system. C7b antibodies were obtained by affinity selection and a phage-display library of Llama single domain antibodies (*Lama glama*).[12] The analysis of the original nucleotide sequence that codes the C7b nanoantibody showed that it has a codon adaptation index (CAI) of 0.74 for *E. coli* cells, as determined using the online server GenScript Rare Codon Analysis Tool.[25] Such a low CAI value indicates the probability of low efficiency of the target protein synthesis, while the values in the range of 0.8–1 indicate a high probability of protein expression in sufficient quantities.[26] In order to increase the expression efficiency, the codon composition of the C7b nucleotide sequence was optimised using online tools: EFM Calculator and GeneOptimizer (see Fig. 1 for plasmid map, Fig. S2† for codon composition before and after optimisation, and Fig. S3† for maps of plasmids used in this study).[19–21] After optimisation, the CAI value increased significantly and achieved a value of 0.93. To increase the efficiency of expression even more, the expressivity tag T7 was included in the construct. The T7 tag is a leader peptide (11 amino acids, MASMTGGQQMG) of the gene10 of bacteriophage T7. The presence of this peptide at the N- or C-terminus significantly increases the yield of the target product.[27] Utilisation of optimised codon composition and the T7 tag for C7b expression resulted in the production yield (calculated per litre of culture medium) of 210–220 mg L^{-1}. According to the literature data, the high yield of sdAbs is considered to be 10–30 mg L^{-1} indicating an ~ 11-fold increase in protein yield in our case. The antibody activity was confirmed by dot blot analysis and enzyme-linked immunosorbent assay (ELISA), as described further.

Preparation and characterisation of silica nanoparticle conjugates

Silica is a very common, transparent in the visible region, non-toxic and versatile matrix used for the development of various therapeutics and diagnostic nanoplatforms,[28–30] and therefore, we chose this material as a model cargo. However, to simplify the detection of the nanoparticles, we used the phosphorescent particles $\{Mo_6I_8\}$@SiO_2 reported in ref. 18 and 31 that can be easily obtained simply by adding a source of Mo_6 cluster (in our case, $(Bu_4N)_2[\{Mo_6I_8\}(NO_3)_6]$) during the synthesis of silica nanoparticles. These particles also have intact surfaces available for further surface functionalisation. In our earlier *in vitro* studies on human epidermoid larynx carcinoma (Hep-2) cells, we have already demonstrated that the cellular uptake/elimination profile, cellular localisation and dark toxicity (*i.e.* in the absence of significant photoirradiation) of both $\{Mo_6I_8\}$@SiO_2 nano- (50 nm) and micro- (500 nm) particles are the same as that of neat silica nanoparticles of the same size.[31] The 50 nm particles (see ESI for TEM images, Fig. S1†) represent amorphous silica doped with $\{Mo_6I_8\}^{4+}$ in the content of 3.0 ± 0.3 mg per 1 g of SiO_2 as determined by ICP-AES analysis.[18] Despite low cluster complex content, the nanoparticles exhibit noticeable cluster-centred red/NIR phosphorescence with a quantum yield of about 12% under light irradiation up to 550 nm.[18] To conjugate the nanoparticles with the targeting antibodies C7b or trastuzumab, a two-step modification was carried out (Scheme 1), similar to that previously reported for

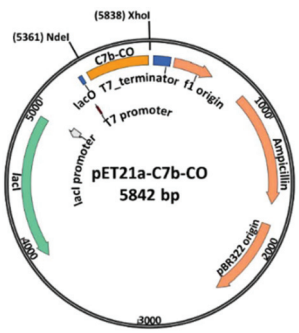

Fig. 1 Map of plasmid pET21a-C7b-CO used for sdAb C7b expression.

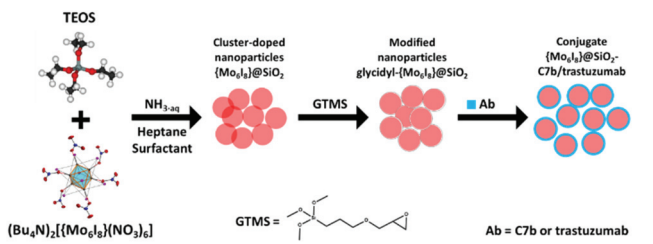

Scheme 1 The synthetic procedure of $\{Mo_6I_8\}$@SiO_2-C7b/trastuzumab.

silica microparticles with green fluorescent protein (GFP).[15] In general, in the first stage, $\{Mo_6I_8\}$@SiO_2 NPs were reacted with (3-glycidyloxypropyl)trimethoxysilane to functionalise the surface of the particles by glycidyl-groups. The solutions of C7b or trastuzumab were then included in the process route by their reaction with an aqueous dispersion of glycidyl-$\{Mo_6I_8\}$@SiO_2 nanoparticles to give stable dispersions of the conjugates: $\{Mo_6I_8\}$@SiO_2-C7b or $\{Mo_6I_8\}$@SiO_2-trastuzumab, respectively.

The qualitative assessment of the activity of synthesised C7b and its conjugate with silica NPs, $\{Mo_6I_8\}$@SiO_2-C7b, was performed by dot blot analysis (Fig. 2A). It can be seen from Fig. 2A that the staining of nitrocellulose paper is observed for all samples, which indicates that there is a selective interaction with the target recombinant protein HER2/neu. Thus, two main conclusions can be drawn: (i) the modified method for C7b production indeed allows the active nanoantibodies to be obtained and (ii) during the conjugation process, the antibodies are indeed attached to the particle surface and they retain a high specific activity. It should be noted that the conjugates obtained using a different ratio of antibody to nanoparticles (3.4 or 6.7 mg of C7b per 10 mg of $\{Mo_6I_8\}$@SiO_2) demonstrated variations in the intensity of staining (Fig. 2A 2 and 7). Since the intensity shows the relative activity, the conjugate that demonstrated the most intensive staining (6.7 mg of C7b per 10 mg of $\{Mo_6I_8\}$@SiO_2) was chosen for further studies.

The quantitative activity was then assessed using ELISA, which demonstrates the effectiveness of the interaction of the antibodies with HER2/neu (Fig. 2B). The figure shows the dependence of the interaction of C7b and $\{Mo_6I_8\}$@SiO_2-C7b *vs.* the quantity of C7b. The data obtained shows that sdAb C7b interacts effectively with HER2/neu up to a concentration of 65 ng mL^{-1}. At the same time, despite a 25% decrease in the affinity for conjugate, overall, the activity persists up to similar concentrations, which confirms the preservation of the antibody structure after conjugation. This reduction in affinity is probably due to the fact that the conjugation technique described here leads to the irregular orientation of sdAb C7b on the nanoparticle surface and therefore provokes antibodies to be partly unfolded, leading to reductions in the efficiency of the interactions of the active site with HER2/neu.[32]

To examine the stability of the cargo, namely the stability of the phosphorescent dopant, the luminescence spectra for aqueous dispersions of initial nanoparticles $\{Mo_6I_8\}$@SiO_2, glycidyl-$\{Mo_6I_8\}$@SiO_2 and conjugates $\{Mo_6I_8\}$@SiO_2-C7b and $\{Mo_6I_8\}$@SiO_2-trastuzumab were recorded (Fig. 3, Table 1).

According to the data obtained, the surface modification of the nanoparticles did not significantly affect the shape of the emission profile and emission maximum (λ). Despite the observable red phosphorescence of the aqueous dispersions, it was, unfortunately, impossible to determine photophysical characteristics such as luminescence quantum yield (Φ) and values of lifetime (τ). However, we were able to determine Φ and τ values for powdered glycidyl-$\{Mo_6I_8\}$@SiO_2 and to compare those to initial $\{Mo_6I_8\}$@SiO_2 particles (Table 1). Therefore, we can conclude, that surface modification leads to only a slight decrease in the luminescence quantum yield with no statistically significant difference in the values of lifetimes. Considering that the clusters are distributed evenly throughout the entire volume of silica particles,[18] the difference in the photophysical characteristics of the materials suggests that the addition of the coatings and conjugates may affect the photoluminescence properties (*e.g.* lead to new paths of non-radiative decay) of the clusters close to the surface of the particles. This effect was not observed for similar but larger (500 nm)

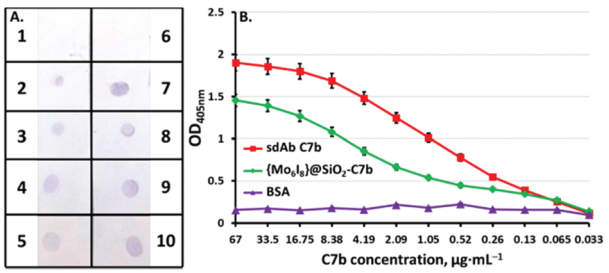

Fig. 2 (A) Qualitative assessment of the activity of C7b and its conjugates with $\{Mo_6I_8\}$@SiO_2 in different ratios of antibody/nanoparticles by dot-blot assay. 1, 6 – BSA (negative control); 2, 7 – $\{Mo_6I_8\}$@SiO_2-C7b (C7b concentration is 3.4 μg and 6.7 μg, respectively) in a different ratio of antibody : nanoparticles (3.4 mg or 6.7 mg of C7b/10 mg of SiO_2, respectively); 3, 8 – sdAb C7b (3.4 μg and 6.7 μg, respectively); 4, 9 – Z500 protein, containing hexahistidine tag (secondary antibody control); 5, 10 – mouse antibody 29F2 (conjugate control). (B) Quantitative determination of the activity of C7b and $\{Mo_6I_8\}$@SiO_2-C7b by ELISA.

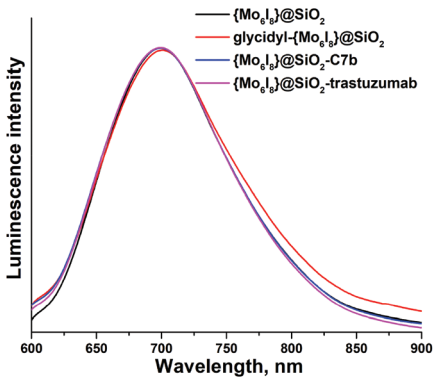

Fig. 3 Normalised emission spectra of initial and modified NPs.

Table 1 The spectroscopic and photophysical parameters of initial and modified NPs

Compound	λ, nm	τ^a, μs	Φ^a
$\{Mo_6I_8\}$@SiO_2 NPs	701	132	0.12
glycidyl-$\{Mo_6I_8\}$@SiO_2	700	139	0.07
$\{Mo_6I_8\}$@SiO_2-C7b	699	—	—
$\{Mo_6I_8\}$@SiO_2-trastuzumab	698	—	—

[a] Measurements were conducted for samples in the solid state.

silica particles, which is likely due to the significantly lesser surface to volume ratio. Indeed, the specific surface area of the nanoparticles was determined to be five-fold of that for microparticles.[18]

In vitro studies

The biological properties of the conjugates *in vitro* were studied on two cell-lines: SKBR3, the human breast cancer cell line that overexpresses HER2 receptor, and Hep-2, the human larynx carcinoma cell line that has low HER2 expression. The MTT assay demonstrated that both conjugates did not show any significant dark cytotoxicity to either of the cell lines within the whole range of the studied concentrations, *i.e.* 1–500 μg mL^{-1} for 72 hours (Fig. 4).

This result agrees with the earlier data on the dark cytotoxicity of $\{Mo_6I_8\}@SiO_2$ [31] and indicates no effect of antibodies on the toxicity profile. Confocal images that were obtained after incubation of both cell lines with the conjugates for 15 min clearly demonstrated a bright red luminescence in SKBR3 cells localised in the perinuclear region and no noticeable luminescence in Hep-2 cells (Fig. 5 and S4†). Thus, the *in vitro* studies confirmed the specific affinity of both conjugates to the HER2/neu receptor, overexpressed by the SKBR3 cells. Moreover, our data demonstrated the internalisation of the particles *within* the SKBR3 cells but not just targeted accumulation on the cellular membrane, which is likely to be driven by the nanoparticles themselves. Indeed, silica particles could easily penetrate through the cell membrane independently with or without biomolecules on the surface[15,33] and, according to the literature, the penetration mechanism of the silica nanoparticles is clathrin dependent/independent endocytosis.[34]

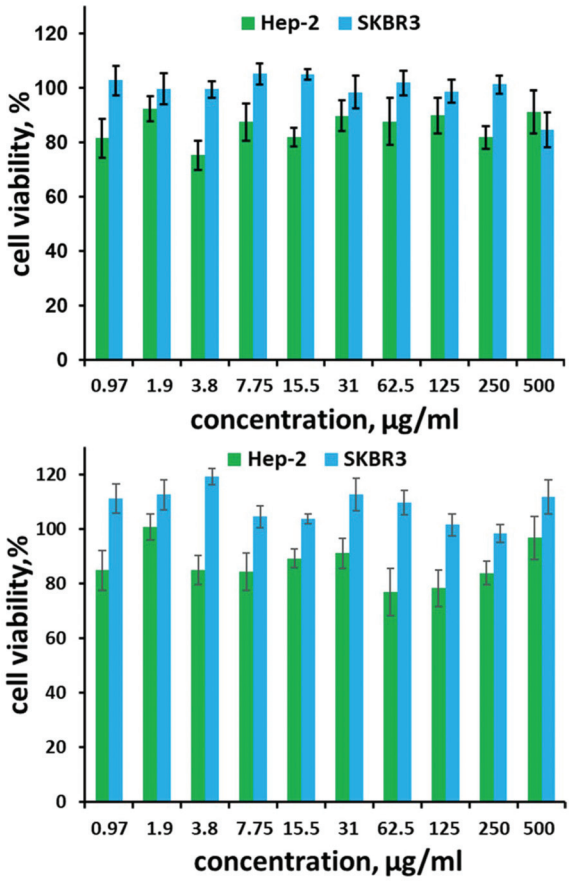

Fig. 4 Cytotoxicity of $\{Mo_6I_8\}@SiO_2$-C7b (up) and $\{Mo_6I_8\}@SiO_2$-trastuzumab (down) evaluated for Hep-2 cells (HER2 low expressed cell line) and SKBR3 cells (HER2-overexpressed cells).

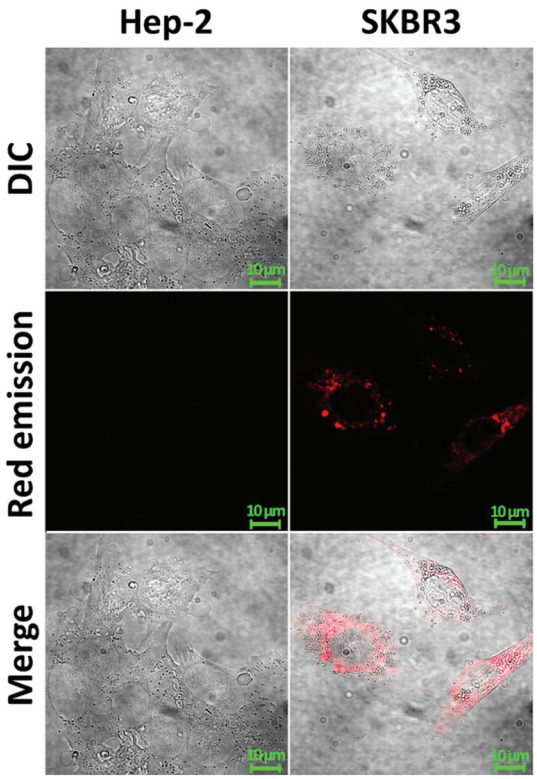

Fig. 5 Confocal microscopic images of Hep-2 and SKBR3 cells incubated with $\{Mo_6I_8\}@SiO_2$-C7b for 15 min.

In vivo studies

To compare the behaviour of the C7b conjugate with that of the trastuzumab conjugate, we studied their accumulation rate in the SKBR3 tumour grafted in mice. To confirm that the administered dose (3.5 mg) of the silica nanoparticle dispersions do not have acute toxicity, 3 female mice of Balb/C line

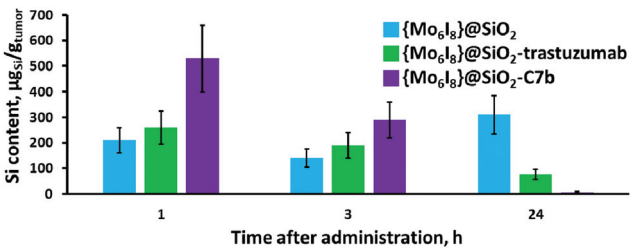

Fig. 6 Silicon content in tumour xenografts determined by ICP-AES.

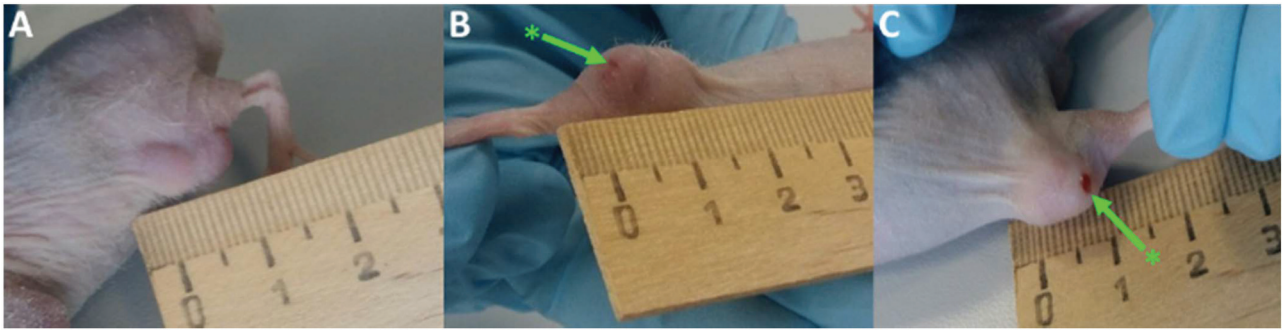

Fig. 7 *In vivo* PDT effect ($\lambda \geq 400$ nm) of $\{Mo_6I_8\}@SiO_2$ on SKBR3 tumour xerograph. (A) Tumour before irradiation. (B) Tumour after first irradiation session. The tumour area had local hyperaemia and oedema. The green arrow indicates a small patch of necrosis. (C) Tumour after third irradiation session. The green arrow indicates increased tissue necrosis.

were injected with the tested materials subcutaneously in the medial thigh area. The mice did not demonstrate any symptoms of intoxication and behaved normally. Thereafter, nine female mice of Nu/J line with xenograft were injected with either neat $\{Mo_6I_8\}@SiO_2$ (negative control) or with the conjugates $\{Mo_6I_8\}@SiO_2$-C7b or $\{Mo_6I_8\}@SiO_2$-trastuzumab (positive control) subcutaneously by 7 consecutive injections at a dose of 0.5 mg each around the tumour. The mice were sacrificed 1, 3 and 24 hours after sample administration and the quantity of the nanoparticles in tumour xenografts was determined using the ICP-AES technique by monitoring the content of silicon atoms in the tissue (Fig. 6).

According to the data obtained (Fig. 6), after 1 hour the conjugate $\{Mo_6I_8\}@SiO_2$-C7b accumulates in the cancerous tissue significantly better than neat $\{Mo_6I_8\}@SiO_2$ or $\{Mo_6I_8\}@SiO_2$-trastuzumab. The silicon amount quantified after 3 hours from injection clearly demonstrated the start of excretion of the conjugates from the tumour xenograft. After 24 h, the amount of the conjugated materials reduce significantly in the tumour; in particular, in the case of $\{Mo_6I_8\}@SiO_2$-C7b, while the amount of $\{Mo_6I_8\}@SiO_2$ remained nearly the same. These results, thus, clearly confirm the selectivity of cluster-doped silica conjugates with both antibodies. However, the higher accumulation efficiency and higher excretion rate of $\{Mo_6I_8\}@SiO_2$-C7b due to the smaller size of the nanobody, compared to the monoclonal antibody, demonstrate its greater potential in the delivery of particular diagnostic (imaging) agents, in which a high rate of accumulation and excretion are required.[35]

Due to the intrinsic ability of $\{Mo_6I_8\}@SiO_2$ to generate singlet oxygen[18,31] we also examined the photodynamic activity of the conjugate with sdAb C7b *in vivo*. A NU/J mouse induced with SKBR3 tumour xerograph having a solid ellipsoidal shape and the size of 1.0 × 0.5 × 0.5 cm was injected with nanoparticle dispersion in a similar fashion as described above. After 1 hour (*i.e.* at the maximum of accumulation), the tumour was irradiated with a halogen lamp (500 W, $\lambda \geq 400$ nm) at a distance of 50 cm for 30 minutes. The whole procedure was repeated twice more with an interval of 3 days. Fig. 7 shows the images of the tumour before and after the PDT. Overall, during and after the PDT, the mouse behaved normally and did not demonstrate any signs of intoxication. After the first irradiation, the tumour area showed signs of local hyperaemia, oedema and a small patch of necrosis at the site that was exposed to light. After the third PDT procedure, the signs of swelling and hyperaemia in tumour were significantly reduced, while tissue necrosis increased. Unfortunately, there was no reduction in the tumour size, although the growth of the tumour was not observed either. Meanwhile, the healthy tissue remained unchanged after the PDT, which suggests the selectivity of particle accumulation within the tumour. Overall, the *in vivo* experiments are generally in agreement with the data obtained *in vitro*, *i.e.* $\{Mo_6I_8\}@SiO_2$ does not have significant dark toxicity, while upon photoirradiation it demonstrates a noticeable photodynamic effect, which initially causes hyperaemia in tumorous tissues and further transforming into necrosis.

Conclusions

In conclusion, the optimised method for the preparation of HER2-specific single-domain antibody C7b resulted in an eleven-fold increase in the antibody yield. Since nanoantibodies have already demonstrated higher potential in anti-cancer therapy and related areas than monoclonal antibodies, their production is of great importance for creating a new type of drug, and therefore, the described method is extremely interesting for pharmaceutical companies, especially due to the fact that it can be easily adopted for industrial-scale production. Moreover, using cluster-doped silica nanoparticles $\{Mo_6I_8\}@SiO_2$ as a model photoactive cargo, we have demonstrated that sdAb C7b can be an effective replacement for conventional mAb (*i.e.* trastuzumab) in applications related to the delivery of drugs, imaging and theranostics agents. Namely, *in vitro* confocal studies showed the significantly higher uptake rate of the silica-based nanoparticles conjugated to C7b or trastuzumab by HER2 overexpressing cell line SKBR3 over those with low expression of HER2—the Hep-2 cells. Notably, our data also demonstrated that the conjugates do

not just accumulate on the cellular membrane after their interaction with a receptor but also penetrate the cell membrane and localise in the perinuclear region of the cells, in a way that is similar to the neat silica nanoparticles. This would be very effective for the delivery of cytostatic/cytotoxic agents directly into the nucleus using silica-based matrices (*e.g.* mesoporous silica nanoparticles loaded with drugs), whereupon C7b facilitates targeted delivery, while the nanoparticles facilitate the uptake and localisation with the cell. The prototype conjugate created in this proof-of-concept study, $\{Mo_6I_8\}$@SiO_2-C7b, confirms the effectiveness of sdAb C7b as an agent for targeted delivery. Moreover, for the first time, this work demonstrated visible light induced *in vivo* photodynamic treatment of cancer on xenografted mice using cluster-containing materials. It should be noted, that despite the modest effect of PDT, it might be increased by using other irradiation types having deeper than visible light tissue penetration, such as infrared irradiation or X-ray.

Conflicts of interest

There are no conflicts to declare.

Acknowledgements

This work was supported by the Russian Science Foundation (grant no. 18-75-10060). OAE thanks the Royal Society for the research grant RSG\R1\180123 and EPSRC grant (EP/R006393/1). The NIIC team thanks the Ministry of Science and Education of the Russian Federation and the Microscopic Centre of the Siberian Branch of the Russian Academy of Sciences for granting access to the microscopic equipment.

References

1 M. J. Adler and D. S. Dimitrov, *Hematol. Oncol. Clin. North Am.*, 2012, **26**, 447–481, DOI: 10.1016/j.hoc.2012.02.013.
2 I. Van Audenhove and J. Gettemans, *EBioMedicine*, 2016, **8**, 40–48, DOI: 10.1016/j.ebiom.2016.04.028.
3 M. Morais and M. T. Ma, *Drug Discovery Today: Technol.*, 2018, **30**, 91–104, DOI: 10.1016/j.ddtec.2018.10.002.
4 *Radiolabeled Monoclonal Antibodies for Imaging and Therapy*, ed. S. C. Srivastava, Springer US, New York, USA, 1988.
5 A. Pinto and M. Pocard, *Pleura Peritoneum*, 2018, **3**(4), 20180124, DOI: 10.1515/pp-2018-0124.
6 D. van Straten, V. Mashayekhi, H. S. de Bruijn, S. Oliveira and D. J. Robinson, *Cancers*, 2017, **9**, 19, DOI: 10.3390/cancers9020019.
7 X. Huang, I. H. El-Sayed, W. Qian and M. A. El-Sayed, *J. Am. Chem. Soc.*, 2006, **128**, 2115–2120, DOI: 10.1021/ja057254a.
8 D. Gao, X. Guo, X. Zhang, S. Chen, Y. Wang, T. Chen, G. Huang, Y. Gao, Z. Tian and Z. Yang, *Mater. Today Bio*, 2020, **5**, 100035, DOI: 10.1016/j.mtbio.2019.100035.
9 P. Bannas, J. Hambach and F. Koch-Nolte, *Front. Immunol.*, 2017, **8**, 1603, DOI: 10.3389/fimmu.2017.01603.
10 G. Hassanzadeh-Ghassabeh, N. Devoogdt, P. De Pauw, C. Vincke and S. Muyldermans, *Nanomedicine*, 2013, **8**, 1013–1026, DOI: 10.2217/nnm.13.86.
11 P. Holliger and P. J. Hudson, *Nat. Biotechnol.*, 2005, **23**, 1126–1136, DOI: 10.1038/nbt1142.
12 K. Even-Desrumeaux, P. Fourquet, V. Secq, D. Baty and P. Chames, *Mol. Biosyst.*, 2012, **8**, 2385–2394, DOI: 10.1039/C2MB25063B.
13 N. Iqbal and N. Iqbal, *Mol. Biol. Int.*, 2014, **2014**, 852748, DOI: 10.1155/2014/852748.
14 K. Even-Desrumeaux, D. Baty and P. Chames, *Mol. Biosyst.*, 2010, **6**, 2241–2248, DOI: 10.1039/c005279e.
15 Y. A. Vorotnikov, T. N. Pozmogova, A. O. Solovieva, S. M. Miroshnichenko, E. V. Vorontsova, L. V. Shestopalova, Y. V. Mironov, M. A. Shestopalov and O. A. Efremova, *Mater. Sci. Eng., C*, 2019, **96**, 530–538, DOI: 10.1016/j.msec.2018.11.056.
16 C. Neaime, M. Amela-Cortes, F. Grasset, Y. Molard, S. Cordier, B. Dierre, M. Mortier, T. Takei, K. Takahashi, H. Haneda, M. Verelst and S. Lechevallier, *Phys. Chem. Chem. Phys.*, 2016, **18**, 30166–30173, DOI: 10.1039/C6CP05290H.
17 O. A. Efremova, M. A. Shestopalov, N. A. Chirtsova, A. I. Smolentsev, Y. V. Mironov, N. Kitamura, K. A. Brylev and A. J. Sutherland, *Dalton Trans.*, 2014, **43**, 6021–6025, DOI: 10.1039/C3DT53126K.
18 Y. A. Vorotnikov, O. A. Efremova, N. A. Vorotnikova, K. A. Brylev, M. V. Edeleva, A. R. Tsygankova, A. I. Smolentsev, N. Kitamura, Y. V. Mironov and M. A. Shestopalov, *RSC Adv.*, 2016, **6**, 43367–43375, DOI: 10.1039/C6RA04321F.
19 B. R. Jack, S. P. Leonard, D. M. Mishler, B. A. Renda, D. Leon, G. A. Suárez and J. E. Barrick, *ACS Synth. Biol.*, 2015, **4**, 939–943, DOI: 10.1021/acssynbio.5b00068.
20 Barrick Lab, EFM Calculator, https://barricklab.org/django/efm/.
21 Thermo Fisher Scientific, GeneOptimizer, https://www.thermofisher.com/ru/ru/home/life-science/cloning/gene-synthesis/geneart-gene-synthesis/geneoptimizer.html.
22 T. Maniatis, E. F. Fritsch and J. Sambrook, in *Molecular Cloning: A Laboratory Manual*, Cold Spring Harbor Laboratory, New York, USA, 1982, pp. 250–251.
23 U. K. Laemmli, *Nature*, 1970, **227**, 680–685, DOI: 10.1038/227680a0.
24 R. Chen, *Biotechnol. Adv.*, 2012, **30**, 1102–1107, DOI: 10.1016/j.biotechadv.2011.09.013.
25 GenScript Biotech Corporation, *GenScript Rare Codon Analysis Tool*, https://www.genscript.com/tools/rare-codon-analysis.
26 R. Jansen, H. J. Bussemaker and M. Gerstein, *Nucleic Acids Res.*, 2003, **31**, 2242–2251, DOI: 10.1093/nar/gkg306.
27 F. W. Studier and B. A. Moffatt, *J. Mol. Biol.*, 1986, **189**, 113–130, DOI: 10.1016/0022-2836(86)90385-2.

28 Z. Xu, X. Ma, Y.-E. Gao, M. Hou, P. Xue, C. M. Li and Y. Kang, *Mater. Chem. Front.*, 2017, **1**, 1257–1272, DOI: 10.1039/C7QM00153C.

29 V. Shirshahi and M. Soltani, *Contrast Media Mol. Imaging*, 2015, **10**, 1–17, DOI: 10.1002/cmmi.1611.

30 J. S. Souris, N.-T. Chen, S.-H. Cheng, C.-T. Chen and L.-W. Lo, in *Cancer Theranostics*, ed. X. Chen and S. Wong, Academic Press, Oxford, UK, 2014, pp. 363–391, DOI: 10.1016/B978-0-12-407722-5.00020-7.

31 A. O. Solovieva, Y. A. Vorotnikov, K. E. Trifonova, O. A. Efremova, A. A. Krasilnikova, K. A. Brylev, E. V. Vorontsova, P. A. Avrorov, L. V. Shestopalova, A. F. Poveshchenko, Y. V. Mironov and M. A. Shestopalov, *J. Mater. Chem. B*, 2016, **4**, 4839–4846, DOI: 10.1039/C6TB00723F.

32 K. Brazhnik, I. Nabiev and A. Sukhanova, *Methods Mol. Biol.*, 2014, **1199**, 129–140, DOI: 10.1007/978-1-4939-1280-3_10.

33 A. Kumari, R. Singla, A. Guliani, A. Acharya and S. K. Yadav, in *Nanoscale Materials in Targeted Drug Delivery, Theragnosis and Tissue Regeneration*, ed. S. K. Yadav, Springer Singapore, Singapore, 2016, pp. 153–172, DOI: 10.1007/978-981-10-0818-4_7.

34 V. Bertelsen and E. Stang, *Membranes*, 2014, **4**, 424–446, DOI: 10.3390/membranes4030424.

35 S. M. Okarvi and H. R. Maecke, in *Peptide Applications in Biomedicine, Biotechnology and Bioengineering*, ed. S. Koutsopoulos, Woodhead Publishing, 2018, pp. 431–483, DOI: 10.1016/B978-0-08-100736-5.00019-3.

